Preprint

Diel Dynamics of Zooplankton Fecal Pellet Flux Revealed by Integrated Optical Observations and Modeling

Yixuan Song[*1], Melissa Omand[1], Colleen A. Durkin[2], Margaret L. Estapa[3], and Deborah K. Steinberg[4]

[1]Graduate School of Oceanography, University of Rhode Island, Narragansett, RI, USA
[2]Monterey Bay Aquarium Research Institute, Moss Landing, CA, USA
[3]School of Marine Sciences, Darling Marine Center, University of Maine, Walpole, ME, USA
[4]Virginia Institute of Marine Science, William & Mary, Gloucester Point, VA, USA

[*]Corresponding author: Yixuan Song, yixuan.song@uri.edu

Scientific Significance Statement

This manuscript describes the first-ever observations of the diel patterns in both fecal pellets and their zooplankton producers from the same in situ imaging platform. The results highlight three distinct zooplankton types, and time and depth variability in the pellets they produce. We use a simple model to show that the observed fecal pellet distributions can be explained by a combination of sinking and diel migration and validate the predictions with diel pellet fluxes from sediment traps. The results also highlight enigmatic species such as appendicularia, that are associated with diel patterns in pellets that are not explained by the model. This study provide insight into the role that different zooplankton play in carbon export and the variability of these processes over hourly timescales.

Data Availability Statement

The data that support the findings of this study are openly available in NASA's SeaBASS archive at https://oceandata.sci.gsfc.nasa.gov/ob/getfile/dd2fe323be_EXPORTS-EXPORTSNP_RR1813_GelCam_20180814-20180909_R1.sb and https://oceandata.sci.gsfc.nasa.gov/ob/getfile/8a0152ccab_EXPORTS-EXPORTSNA_JC214_GelCam_20210504-20210509_R1.sb.
UVP data is available at https://ecotaxa.obs-vlfr.fr/prj/1591 on EcoTaxa.

Abstract

The contribution of sinking fecal pellets to the biological carbon pump depends on pellet properties, producer abundance, and the depth and timing of pellet production, which can be modulated by diel vertical migration. We examined diel variability in zooplankton fecal pellet flux in the subarctic Northeast Pacific using two image-based tools: the Underwater Vision Profiler (UVP5) and upward-facing cameras (GelCam) on a surface-tethered sediment trap array. Three fecal pellet types were classified across both platforms, enabling complementary estimates of pellet abundance, modeled carbon content, and flux. Daily composites revealed distinct diel patterns in three zooplankton types (crustacea, salps, and appendicularia) and their associated pellet flux. A simple model linking zooplankton vertical migration and pellet production, sinking, and attenuation reproduced the observed temporal variability for the migrators. A compelling diel pattern in appendicularian pellets warrants further investigation. Together, these results highlight how diel behavior and physiology impact vertical carbon transport.

Keywords: Biological carbon pump, fecal pellet, zooplankton, diel vertical migration, particle export

Introduction

Zooplankton play an important role in the biological carbon pump by packaging organic matter into dense, compact pellets that can sink rapidly (Shatova et al. 2012; Turner 2015). Many zooplankton taxa also migrate vertically on a diel and/or seasonal basis which can modulate or enhance their contribution to carbon export through the 'active' or 'migratory' pump (Steinberg et al. 2000; Archibald et al. 2019; Clements et al. 2025). The relative importance of different zooplankton groups, and how their physiological and migratory patterns affect fecal-pellet export flux and efficiency is an area of active research due in part to spatial and temporal variability in zooplankton community composition (Steinberg and Landry 2017). As a result, estimates of the overall contribution of fecal pellets vary widely across regions, seasons, and depths, and represent between 30% to 98% of the total particulate organic carbon (POC) flux (Turner 2015).

Fecal pellets produced by different zooplankton species differ in morphology, composition, and sinking speed (Saba and Steinberg 2012; Wilson et al. 2013; Li et al. 2022). For example, crustaceans produce long and cylindrical pellets (Fowler and Small 1972; Yoon et al. 2001; Pauli et al. 2021), whereas salp pellets are typically larger and tabular shaped (Bruland and Silver 1981; Yoon et al. 2001; Durkin et al. 2021). Compact ellipsoid pellets, often attributed to appendicularia (Wilson et al. 2013) and 'mini pellets' (<50 μm) produced by microzooplankton or nauplii also contribute to export (Gowing and Silver 1985). Compounding this morphological variability, different zooplankton groups may produce (Wilson et al. 2008; Li et al. 2022; Sharpe et al. 2025), and consume (Poulsen and Kiørboe 2005; Poulsen and Iversen 2008) pellets at different depths in the water column depending on their migratory and physiological rhythms.

Diel vertical migration (DVM) has been widely studied using echo sounders (Parra et al. 2019; Wiebe et al. 2023) and acoustic doppler current profilers (Cisewski et al. 2010; Inoue et al. 2016) highlighting the diversity of DVM patterns across different physical environments. Studies that utilize net sampling in discrete depth intervals reveal that much of this variability is also taxon-specific. Some taxa, such as salps, migrate hundreds of meters each day (e.g., Steinberg et al. 2023), whereas others, such as appendicularia, are non-migrating and include species that maintain their location in deep layers (e.g., Tomita et al. 2003). Other studies examined diel differences in fecal pellet production or flux, typically using paired day-and-night net sampling or fecal pellet production experiments (Youngbluth et al. 1989; Urban-Rich et al. 1999; Stamieszkin et al. 2021; Sharpe et al. 2025). However, since these approaches are typically limited to 12-hour day-and-night pairings, we do not yet have direct measurements of how, or if, fecal pellet fluxes co-vary with DVM over hourly timescales.

Technological advancements in image-based tools that segment images into regions of interest (ROIs) corresponding to individual particles, enable high-resolution in situ observations of zooplankton and pellets. Upward-facing, time-lapse camera systems (e.g., GelCam; Song et al. 2025) allow for quantification of sinking particle flux at sub-hourly timescales. Other imaging instruments, such as the UVP5 (Picheral et al. 2010) can be used to estimate particle fluxes by coupling particle size spectra with sinking-speed models and high-temporal-resolution profiling deployments (Guidi et al. 2008).

Here we combined UVP casts (123 casts, 292,662 ROIs), GelCam deployments (3,267 images, 703,234 ROIs), and modeling, to examine diel variations in fecal-pellet producers, and

morphologically-defined pellet concentration and flux during the EXport Processes in the Ocean from Remote Sensing (EXPORTS) North Pacific field campaign. Together, these datasets revealed distinct diel variations among three fecal-pellet groups: long, tabular, and ellipsoid pellets. To interpret these observations, we examine the diel vertical migration behavior of their likely producers (crustacea, salps, and appendicularia, respectively) and developed a simple model linking DVM with particle production, sinking, and attenuation to reproduce the main features of the observed diel patterns. Together, these findings emphasize the role of taxon-specific behaviors and fecal pellet characteristics on short-term variability in the biological carbon pump and the value of high-resolution observations that can resolve dynamics on diel (and shorter) time scales.

Materials and Methods

Cruises and sampling platform

The North Pacific EXPORTS campaign was conducted near Ocean Station Papa (50°N, 145°W) from August to September 2018 (Siegel et al. 2021). In this manuscript, we focus upon two datasets: the UVP profiles from the R/V *Sally Ride*, and the timeseries of particle flux from the GelCam on the drifting sediment trap array deployed from the R/V *Roger Revelle* (Figure 1). The methodological and data analysis steps for each system are detailed below.

Underwater vision profiler sampling

A UVP5 system (Picheral et al. 2010) was mounted on the CTD–Rosette and operated during the downcast of each CTD profile, illuminating and imaging a nominal volume of 1.06 L of water at a frame rate of approximately 6 Hz. The effective sampling volume within each depth bin was adjusted in post-processing based on the instantaneous CTD downcast speed. Images of all

particles larger than approximately 1 mm in equivalent spherical diameter were segmented for subsequent classification using EcoTaxa (Picheral et al. 2017). Each segmented ROI corresponded to a single classified particle with associated metadata including depth, timestamp, and morphology. Classification was performed using EcoTaxa's built-in Random Forest model, followed by manual validation. The classified dataset is publicly available through EcoTaxa (https://ecotaxa.obs-vlfr.fr/prj/1591).

Particle classification through EcoTaxa identified 68 morphological categories, including zooplankton and non-living particles. Of these, three were fecal-pellet classes: long, tabular, and ellipsoid fecal pellets. Corresponding producer taxa were also identified. Long fecal pellets are typically produced by crustaceans (Fowler and Small 1972; Wilson et al. 2008; Pauli et al. 2021; Perhirin et al. 2025b), which in our analysis were mostly copepods, euphausiids, and amphipods. Large, tabular fecal pellets (usually referred to as salp pellets) are produced primarily by salps (Bruland and Silver 1981; Yoon et al. 2001), though doliolids can also generate visually similar fecal pellets (Patonai et al. 2011). As doliolid abundance was comparatively low at our study site (i.e., equal to <4% of salp abundance as imaged by UVP) and the size of tabular pellets imaged by the UVP were consistent with those collected in our on-board salp fecal pellet production experiments (Stamieszkin et al. 2021, Steinberg et al. 2023) we assumed salps are the primary producer of tabular pellets. To improve classification accuracy, we applied an additional screening to the ellipsoid fecal pellet category based on UVP morphological classes to remove living particles and mislabeled objects (Figure S1). Observed ellipsoid fecal pellets are likely produced by appendicularia (Dagg et al. 2014; Li et al. 2022; Wilson et al. 2013). Table 1 summarizes numbers of the three fecal pellet groups and their corresponding producers.

All classified particles were binned into one-hour time intervals and 10-m depth intervals from 0 to 500 m. The local, hourly-binned time of day distribution is shown in supplemental materials (Figure S2). Because certain time periods were undersampled during the campaign, a two-hour temporal smoothing filter was applied. Of 143 casts, 20 profiles were removed because they were test casts, or had anomalously high particle concentrations (Figure S3).

Gel trap sampling and GelCam imaging

A surface-tethered trap (STT) array equipped with gel traps (Durkin et al. 2021) and GelCam system was deployed during three sequential collection periods: Deployment 1 (August 15–21), Deployment 2 (August 24–28), and Deployment 3 (August 31–September 5). GelCams were mounted at the three shallowest depths (105, 155, and 205 m). The GelCam is a low-cost, upward-facing 8-megapixel camera that captures images of the gel layer at the base of a sediment trap every 20 minutes. Image sequences were processed to detect, track, and classify individual particles (>170 μm ESD) through time. Particulate organic carbon (POC) flux was then computed by summing the carbon content estimated for each detected particle. For details, see Song et al. (2025).

Results

Crustacea and long pellets

Crustaceans observed by the UVP (n = 11,239) binned into an hourly, depth-resolved 24 h composite, exhibited clear diel vertical migration (Figure 2a), accumulating above 50 m at night

and descending to ~100 m during daylight, with abundances decreasing sharply below 100 m. Consistent with this pattern, long fecal pellets (n = 6,410) were also concentrated above 100 m, and attenuated strongly with depth. The time-averaged long fecal pellet concentration peaked at 40 m, at 0.019 counts L^{-1}, decreased to 0.0061 counts L^{-1} at 100 m, and further declined to 3.4×10^{-4} counts L^{-1} at 150 m. The long pellets also showed diel variability, with the highest concentrations near 50 m observed from dusk through dawn (roughly corresponding to the increased abundance of crustacea at that depth during night). The diel patterns of long pellets deeper (between 75 and 100m) shows an asymmetrical time-lagged pattern, reaching a peak at 20:00 and a minimum at around 08:00.

The sharp decrease in pellet concentration with increasing depth is attributed to a combination of rapid remineralization/consumption and disaggregation of the fragile morphology that cause pellet fragments to be classified in a different category (Durkin et al. 2021). We quantify this depth-attenuation in pellet concentration by fitting a 'Martin curve' functional form:

$$C_z = C_0 \left(\frac{z}{z_0}\right)^{-b},$$

where z_0 represents a reference depth (z_0 = 100 m), C_z and C_0 are the corresponding particle concentrations, and b describes the rate of concentration attenuation in depth. Assuming that these particles are sinking at rate w, we can apply a scaling to estimate the temporal attenuation rate R according to

$$R = \frac{b}{z} \cdot w.$$

Taking w = 100 m day^{-1} (representing the long pellet sinking rate from Perhirin et al. 2025a) and z = 100 m, we obtain a temporal attenuation rate of R = 6.0 day^{-1} (see supplemental materials for

the complete equations). This loss rate is higher than what is expected by microbial remineralization alone, and we emphasize that it is likely a combination of 'true' consumption losses and 'apparent' losses by fragmentation that either fall below the detection limit of the UVP or are classified in a different morphological category as suggested in Durkin et al. (2021).

Salps and tabular pellets

Despite the limited UVP detection numbers (n = 405), salps also showed a diel migration in the daily composite, with highest abundances in the upper 100 m at night, and virtually zero observations in the surface during day. Detections were evident at deeper depths during the migration shoulders near dawn and dusk (Figure 2b). The lower overall concentrations during daytime suggest that many individuals were migrating deeper than the maximum UVP depth of 500 m (consistent with diel, discrete-depth net tow measurements from Steinberg et al. 2023). Tabular pellets (n = 409) showed a strikingly similar pattern, with peak concentrations occurring in early morning and descending downwards. Though unlike the animal abundance, the tabular pellet abundance is asymmetrical, with a downward plume shape, and peak in deep concentration between 17:00 and 22:00.

Appendicularia and ellipsoid pellets

Appendicularia detected by the UVP were found primarily below 300 m, with a fairly uniform concentration of 2 to 4×10^{-3} counts L^{-1} between 350 and 500 m (Figure 2c). Consistent with what is known of their ecology they did not exhibit diel migration. Their compact ellipsoid pellets were also detected primarily at depth, but unlike the animals, were concentrated in a tight layer around

375 m and showed a marked diel cycle, varying from ~0.5×10^{-3} counts L^{-1} during the day, and reaching >2.5×10^{-3} counts L^{-1} near midnight (Figure 2f).

Sinking pellet fluxes from GelCam

Among the three fecal pellet types analyzed here, only the long fecal pellets were statistically abundant enough in the GelCam images to bin into hourly averages. The tabular pellets were too rare (Figure 2h), and the ellipsoid pellets occurred deeper than the deepest GelCam. Sinking long pellet arrival times were binned into one-hour intervals and smoothed using a two-hour filter. At STT1 (105 m), the long fecal pellet flux was at a minimum (<1 mmol C m^{-2} day^{-1}) at 04:00 and peaked at approximately 3 mmol C m^{-2} day^{-1} between 21:00 and 22:00 (Figure 2g), with a time average of 1.79 mmol C m^{-2} day^{-1}. At STT2 (155 m), the long pellet flux was much lower, with an average of 0.18 mmol C m^{-2} day^{-1} and no discernable diel pattern. We compared the long pellet patterns to other particle types such as aggregates and found no diel patterns at either trap depth (Figure S4). A two-point attenuation rate (between 105 and 155 m) estimated from the time-averaged GelCam fluxes yielded an attenuation exponent b of 4.6 day^{-1}, similar to that obtained from the UVP observations.

Modeling the interaction of diel vertical migration and pellet sinking

To explore the diel patterns in fecal pellet abundance and the connections to DVM, we developed a simple model to simulate the two diel migrating pellet producers (Crustacea and Salps/Doliolids), pellet production and sinking (Figure 3). Diel migrations by these two taxa were modeled with a half cosine shape (Figure 3a,d). Crustacea reached a noon-time mean depth of 65 m based on the UVP observations (Figure 2) and echo sounder data (120 and 200 kHz echograms, Figure S5).

Modeled salps migrated to a mean of 450 m, consistent with the range in Steinberg et al. (2023). Next, we assumed constant fecal pellet production rates, attenuation, and sinking speeds for both pellet types. Long fecal pellets were assigned a slower sinking speed of 100 m day^{-1}, consistent with Perhirin et al. (2025a), while tabular pellets were set at 500 m day^{-1}, characteristic of salp fecal pellets (Bruland and Silver 1981). A constant attenuation rate of 0.004 min^{-1} (5.8 day^{-1}) was applied to long fecal pellets based on the scaling described above. Tabular pellets were attenuated at half this rate, given their large size.

Overall, the model shows good agreement between the modeled and measured fecal pellet abundance. For long fecal pellets, the model reproduced the temporal asymmetry, with a descent in the lower range of the pellet layer in late afternoon – lagged after the descent of the producers (compare the modeled results in Figure 3b with the observations in Figure 3c). The modeled pellet abundance along the red dashed line at 100 m is shown in the inset of Figure 3b - highlighting the phase lag. This pattern agrees quite well with both the UVP abundance at 100 m (black line) and the GelCam flux (gray line) on the inset of Figure 3c – both displaying a minimum near 05:00 and a maximum at 19:00 and 21:00 respectively. The similarity in shape between the diel pattern in observed pellet flux with observed and modeled pellet abundance further suggests that the assumption of steady sinking is valid over this particle type and time scale.

The modeled tabular pellet abundances (Figure 3e) also captured the observed asymmetry – the combination of zooplankton diel vertical migration and pellet sinking rates produced a pellet plume that followed the animals in the morning descent. In the afternoon, the fast-sinking rate of the

particles offsets the effect of upward migration, causing a marked reduction in pellet abundance during the migration upward at night (compare Figure 3e with 3f).

Discussion

This study resolves diel variability in fecal pellet–mediated POC flux and examines how zooplankton DVM and particle sinking jointly shape carbon transport. Combining UVP5 and GelCam observations with a simple migration–sinking model, we show that diel POC flux signals arise from interactions between migration of zooplankton fecal pellet producers and pellet sinking. Together, the observations and model indicate that the migratory pump is not a single mechanism, but a set of particle-specific pathways in which producer behavior, fecal pellet properties, and sinking rates determine whether migration efficiently enhances export or contributes to attenuation through particle transformation.

There are limitations in this observational work that should be acknowledged. Variability in the timing of UVP casts generated somewhat more sample effort during the day versus night (Figure S2). Overall, the UVP and GelCam both likely under-sampled the pellets since many were probably smaller than the detection limits of the instruments. For example, microscope analysis of the gels revealed that only 1% of the long pellets had an ESD greater than the detection threshold of the UVP images (particles >1 mm). For this reason, we advise against any interpretation of production rates from the ratio of pellets to producers, since we believe the pellets were undercounted relative to the producers. Finally, the model framework does not encompass the diversity of organisms within each major taxon, variations in grazing and remineralization, or diel

variability in fecal pellet production rates–as proposed or observed in other ecosystems (Glooschenko et al. 1972; Lebouteiller and Herbland 1982; Tarrant et al. 2021).

UVP observations of the long fecal pellets showed a descent in the lower range of distribution in late afternoon, descending below 100m (the depth of the shallowest sediment trap). This pattern was reproduced by the model, suggesting that it may have arisen from a combination of sinking and migration of crustacean zooplankton. The high depth-attenuation in the long pellets may result from their nutrient-rich composition, favorable for bacterial colonization. Iversen and Ploug (2010) indicate that additional attenuation may come from zooplankton reprocessing, as migrating zooplankton can graze on or repackage long fecal pellets during sinking. Another plausible explanation is fragmentation. Fragmentation can occur under low turbulence (Briggs et al. 2020) or even laminar flow conditions (Song et al. 2023). Given their elongated morphology and susceptibility to degradation, long fecal pellets are prone to fragmentation, producing smaller particles that may be reclassified as other particle types or be too small to be detected by instruments such as the UVP5 and GelCam. The attenuation rates reported here therefore reflect not only remineralization, but also particle transformation and physical processes affecting particle transfer efficiency.

In contrast to the fragile, and quickly attenuating long pellets, tabular fecal pellets associated with salps represent a strong, fast export pathway within the migratory pump (Durkin et al. 2021; Steinberg et al. 2023). Their large size, high density, and rapid sinking efficiently transport surface-derived carbon below the mixed layer. The simplified model reproduced the observed depth-

dependent concentration and diel asymmetry pattern, with a maximum near-surface abundance at dawn, and a plume of pellets that descended rapidly throughout the day.

Intriguingly, ellipsoid pellets were most abundant in a narrow layer between 350 and 400 m which was in the upper range of the distribution of their assumed appendicularian producers. Durkin et al. (2021) suggested that fecal pellet abundance at these depths may also be influenced by diel variability in grazing behavior, thus one possible hypothesis is that other migrators such as copepods intercept or consume ellipsoid fecal pellets while at depth, leading to reduced daytime abundance. This hypothesis supports the idea that zooplankton fecal pellets may contribute to carbon export through passive sinking while being concurrently attenuated by active, behavior-driven zooplankton processes (Steinberg and Landry 2017). This pattern likely represents a complementary signal of reprocessing and recycling of sinking particles that applies broadly beyond appendicularian fecal pellets. In this context, the observed diel signal is best interpreted as behaviorally-mediated export attenuation rather than enhancement. Appendicularia are not attenuators to carbon export, but interception or consumption of their fecal pellets, with potential upward transport, may reduce the effective transfer depth and residence time of sinking carbon.

Together, the observations and model show that diel cycling strongly influences zooplankton-mediated fecal pellet flux in the upper ocean. Differences in vertical migration depth and fecal pellet sinking rate and attenuation generate distinct temporal signals among fecal pellet types, leading to contrasting contributions to carbon export. These results demonstrate that resolving sub-daily dynamics is critical for understanding how animal behavior and particle properties jointly regulate vertical carbon transport.

Acknowledgements

Data collected through this project was supported by NASA Grants 80NSSC17K0662 and 80NSSC21K0015 to M.L.E., M.M.O. and C.A.D., and 80NSSC17K0654 to D.K.S.. Postdoctoral support for Y.S. was provided through Simons Foundation and Ocean Twilight Zone projects, subcontracted through Woods Hole Oceanographic Institution.

We acknowledge Dr. Andrew McDonnell as the owner of the UVP dataset analyzed in this study, which is publicly available through EcoTaxa, and Jessica Pretty and Rachel Lekanoff for manual validation of UVP particle classifications in EcoTaxa.

We wish to thank Drs. Stephanie H O'Daly, Dr. Ken Buesseler, Dr. Nils Haentjens, Dr. Dave Siegel, and the EXPORTS team for assistance with data collection, their helpful discussions and constructive recommendations. We are also grateful to captains and crew of the R/V *Revelle*, R/V *Sally Ride*, and R/V *James Cook*.

We acknowledge the use of AI tools for grammar refinement.

Tables and Figures

Table 1. Number of fecal pellets and their likely producers observed by UVP5.

fecal pellets	long pellets	tabular pellets	ellipsoid pellets
	6,410	409	1,284
likely fecal pellet producers	crustacea	salps	appendicularia
	11,239	391	3,264

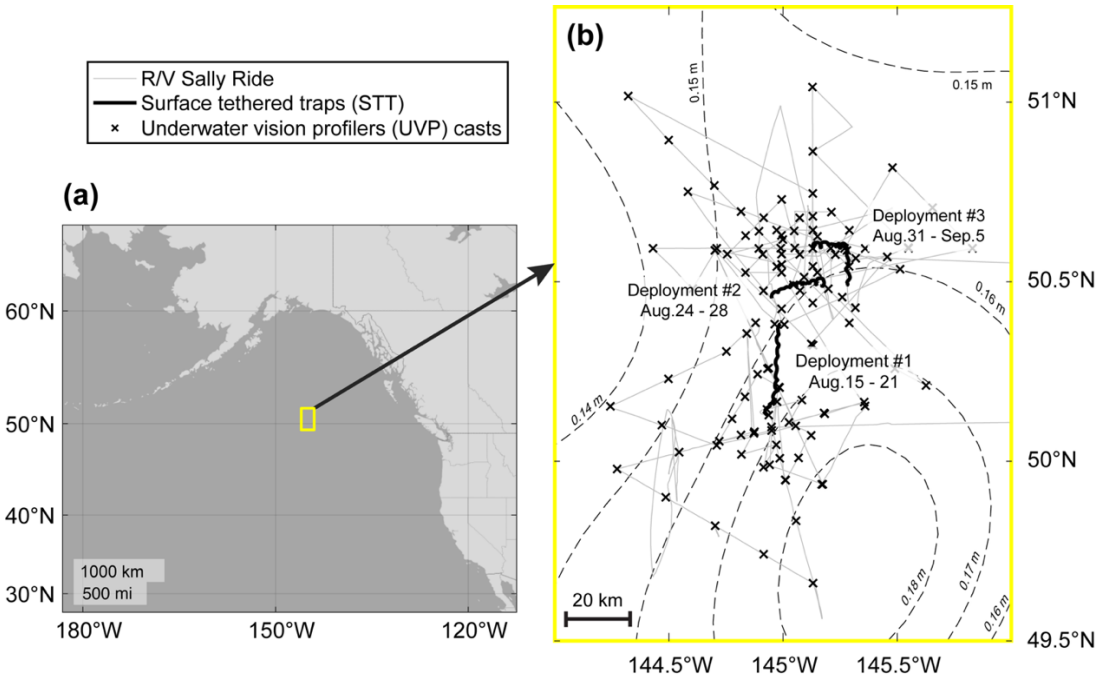

Figure 1: Study site and sampling platforms during the EXPORTS North Pacific field campaign. The field program was conducted at Ocean Station Papa (50°N, 145°W) in the subarctic Northeast Pacific Ocean during summer 2018. The thin gray line denotes the cruise track of the R/V *Sally Ride*, while the three thick gray lines represent the trajectories of the surface-tethered sediment traps deployed from the R/V *Roger Revelle*. Cross symbols mark the locations of 143 UVP casts conducted from the R/V *Sally Ride*. Dashed contours show the mean sea surface height anomaly averaged between 14 August and 13 September 2018.

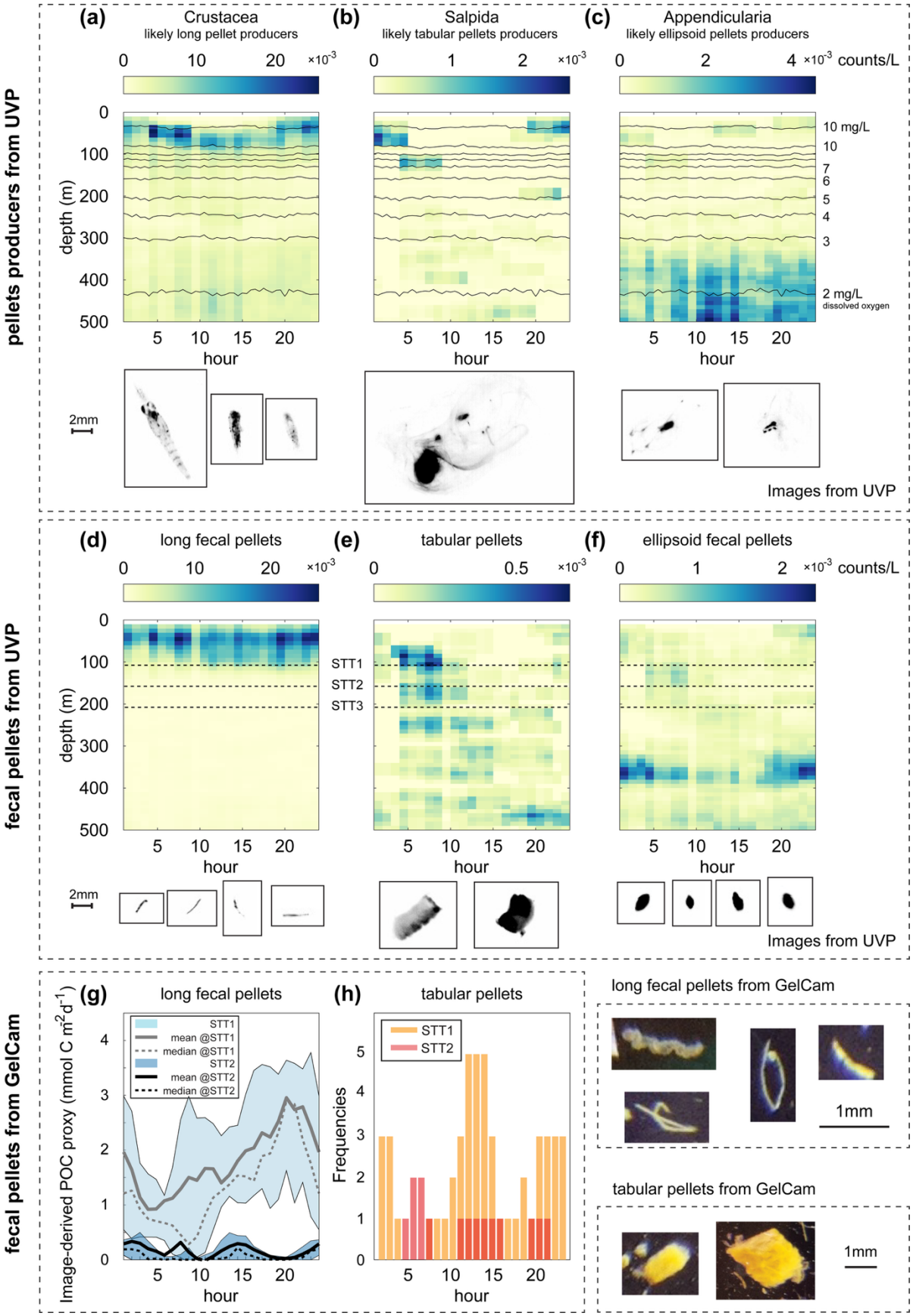
pellets producers from UVP
(a) Crustacea
likely long pellet producers
(b) Salpida
likely tabular pellets producers
(c) Appendicularia
likely ellipsoid pellets producers
counts/L
depth (m)
hour
10 mg/L
2 mg/L
dissolved oxygen
2mm
Images from UVP
fecal pellets from UVP
(d) long fecal pellets
(e) tabular pellets
(f) ellipsoid fecal pellets
STT1
STT2
STT3
fecal pellets from GelCam
(g) long fecal pellets
(h) tabular pellets
Image-derived POC proxy (mmol C m^{-2}d^{-1})
mean @STT1
median @STT1
mean @STT2
median @STT2
Frequencies
long fecal pellets from GelCam
tabular pellets from GelCam
1mm

361

Figure 2. Daily averaged abundance of fecal pellets and their producers (a–f) from UVP5, and daily averaged time series of particulate organic carbon (POC) flux across depths and particle types (g–h) from GelCam. Panels (a–c) show the abundance of (a) crustaceans, (b) salps, and (c) appendicularia. Panels (d–f) present the corresponding fecal pellet types: (d) long, (e) tabular, and (f) ellipsoid fecal pellets. Example images of each zooplankton taxon or particle type are displayed below the corresponding color maps. Contours in the upper panels indicate dissolved oxygen concentration (mg L^{-1}). Panel (g) shows the image-derived POC proxy of long fecal pellets measured by GelCam at STT 1 (105 m) and STT 2 (155 m). The upper and lower boundaries of the patches represent 75th and 25th percentile of the samples, with the mean and median shown as solid and dashed lines. Panel (h) displays frequency histograms of tabular pellets. Data from STT 3 (205 m) are excluded because of insufficient observations. Uncertainty in the coefficient of variation is shown in Figure S6.

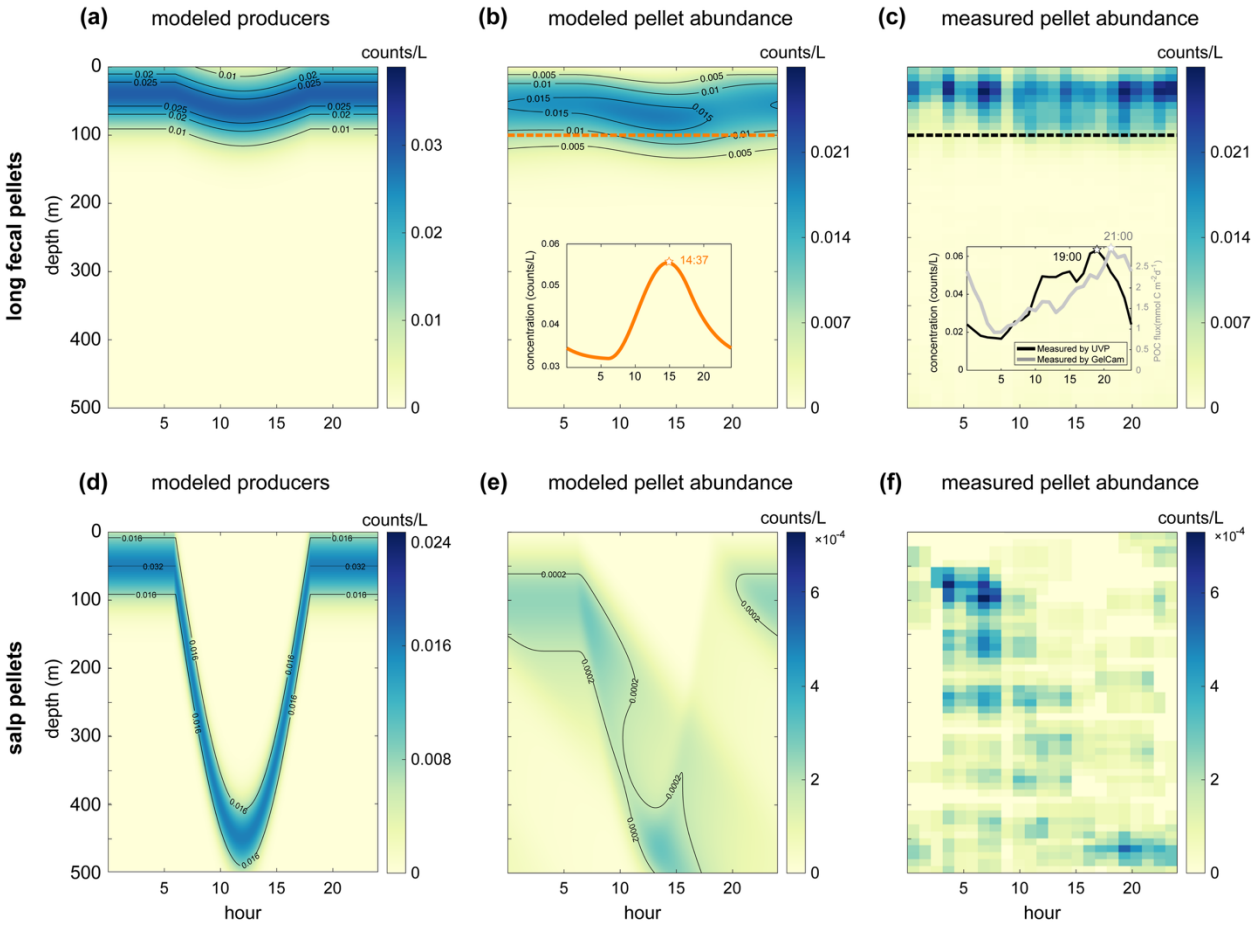

375

376 Figure 3: Modeled DVM patterns and fecal pellet abundance. Panels (a) and (b) show the simulated
377 DVM of crustacea and the corresponding distribution of long fecal pellets, with its inset panels
378 showing the modeled particle flux at 100 m. Panel (c) and its subpanels compare the observed
379 abundance and modeled flux at 100 m. The lower panels depict the simulated migration of salps
380 and compare the modeled and observed abundances of tabular fecal pellets.

381

382

References

Archibald, K. M., D. A. Siegel, and S. C. Doney. 2019. Modeling the Impact of Zooplankton Diel Vertical Migration on the Carbon Export Flux of the Biological Pump. Global Biogeochem Cycles 33: 181–199. doi:10.1029/2018GB005983

Briggs, N., G. Dall'Olmo, and H. Claustre. 2020. Major role of particle fragmentation in regulating biological sequestration of CO2 by the oceans. Science (1979) 367: 791–793. doi:10.1126/science.aay1790

Bruland, K. W., and M. W. Silver. 1981. Sinking rates of fecal pellets from gelatinous zooplankton (Salps, Pteropods, Doliolids). Mar Biol 63: 295–300. doi:10.1007/BF00395999

Cisewski, B., V. H. Strass, M. Rhein, and S. Krägefsky. 2010. Seasonal variation of diel vertical migration of zooplankton from ADCP backscatter time series data in the Lazarev Sea, Antarctica. Deep Sea Research Part I: Oceanographic Research Papers 57: 78–94. doi:10.1016/j.dsr.2009.10.005

Clements, D. J., K. Stamieszkin, D. Bianchi, L. Blanco-Bercial, N. R. Record, R. B. Rodriguez-Perez, and A. E. Maas. 2025. Active Carbon Transport by Diel Vertical Migrating Zooplankton: Calculated and Modeled, but Never Measured. Ann Rev Mar Sci. doi:10.1146/annurev-marine-121422-015330

Dagg, M. J., G. A. Jackson, and D. M. Checkley. 2014. The distribution and vertical flux of fecal pellets from large zooplankton in Monterey bay and coastal California. Deep Sea Research Part I: Oceanographic Research Papers 94: 72–86. doi:10.1016/j.dsr.2014.09.001

Durkin, C. A., K. O. Buesseler, I. Cetinić, M. L. Estapa, R. P. Kelly, and M. Omand. 2021. A Visual Tour of Carbon Export by Sinking Particles. Global Biogeochem Cycles 35. doi:10.1029/2021GB006985

Fowler, S. W., and L. F. Small. 1972. Sinking rates of euphausiid fecal pellets. Limnol Oceanogr 17: 293–296. doi:10.4319/lo.1972.17.2.0293

Glooschenko, W. A., H. Curl Jr., and L. F. Small. 1972. Diel Periodicity of Chlorophyll a Concentration in Oregon Coastal Waters. Journal of the Fisheries Research Board of Canada 29: 1253–1259. doi:10.1139/f72-191

Gowing, M. M., and M. W. Silver. 1985. Minipellets: A new and abundant size class of marine fecal pellets. J Mar Res 43: 395–418. doi:10.1357/002224085788438676

Guidi, L., G. A. Jackson, L. Stemmann, J. C. Miquel, M. Picheral, and G. Gorsky. 2008. Relationship between particle size distribution and flux in the mesopelagic zone. Deep Sea Research Part I: Oceanographic Research Papers 55: 1364–1374. doi:10.1016/j.dsr.2008.05.014

Inoue, R., M. Kitamura, and T. Fujiki. 2016. Diel vertical migration of zooplankton at the <scp>S</scp> 1 biogeochemical mooring revealed from acoustic backscattering strength. J Geophys Res Oceans 121: 1031–1050. doi:10.1002/2015JC011352

Iversen, M. H., and H. Ploug. 2010. Ballast minerals and the sinking carbon flux in the ocean: carbon-specific respiration rates and sinking velocity of marine snow aggregates. Biogeosciences 7: 2613–2624. doi:10.5194/bg-7-2613-2010

Lebouteiller, A., and A. Herbland. 1982. Diel variation of chlorophyll-a as evidenced from a 13-day station in the equatorial Atlantic-ocean. Oceanologica Acta 5: 433–441.

Li, J. and others. 2022. Zooplankton Fecal Pellet Characteristics and Contribution to the Deep-Sea Carbon Export in the Southern South China Sea. J Geophys Res Oceans 127. doi:10.1029/2022JC019412

Parra, S. M., A. T. Greer, J. W. Book, A. L. Deary, I. M. Soto, C. Culpepper, F. J. Hernandez, and T. N. Miles. 2019. Acoustic detection of zooplankton diel vertical migration behaviors on the northern Gulf of Mexico shelf. Limnol Oceanogr 64: 2092–2113. doi:10.1002/lno.11171

Patonai, K., H. El-Shaffey, and G.-A. Paffenhofer. 2011. Sinking velocities of fecal pellets of doliolids and calanoid copepods. J Plankton Res 33: 1146–1150. doi:10.1093/plankt/fbr011

Pauli, N.-C. and others. 2021. Krill and salp faecal pellets contribute equally to the carbon flux at the Antarctic Peninsula. Nat Commun 12: 7168. doi:10.1038/s41467-021-27436-9

Perhirin, M., O. Aumont, F. Maps, and S.-D. Ayata. 2025a. Meta-analysis of the role of zooplankton faecal pellets in ocean carbon export flux. ICES Journal of Marine Science 82. doi:10.1093/icesjms/fsaf180

Perhirin, M., L. Vilgrain, G. Perrin, C. Lalande, M. Picheral, F. Maps, and S.-D. Ayata. 2025b. Identifying zooplankton fecal pellets from in situ images. J Plankton Res 47. doi:10.1093/plankt/fbae078

Picheral, M., S. Colin, and J. O. Irisson. 2017. EcoTaxa, a tool for the taxonomic classification of images. http://ecotaxa.obs-vlfr.fr.

Picheral, M., L. Guidi, L. Stemmann, D. M. Karl, G. Iddaoud, and G. Gorsky. 2010. The Underwater Vision Profiler 5: An advanced instrument for high spatial resolution studies of particle size spectra and zooplankton. Limnol Oceanogr Methods 8: 462–473. doi:10.4319/lom.2010.8.462

Poulsen, L., and M. Iversen. 2008. Degradation of copepod fecal pellets: key role of protozooplankton. Mar Ecol Prog Ser 367: 1–13. doi:10.3354/meps07611

Poulsen, L., and T. Kiørboe. 2005. Coprophagy and coprorhexy in the copepods Acartia tonsa and Temora longicornis: clearance rates and feeding behaviour. Mar Ecol Prog Ser 299: 217–227. doi:10.3354/meps299217

Saba, G. K., and D. K. Steinberg. 2012. Abundance, Composition and Sinking Rates of Fish Fecal Pellets in the Santa Barbara Channel. Sci Rep 2: 716. doi:10.1038/srep00716

Sharpe, K. N., D. K. Steinberg, and K. Stamieszkin. 2025. The Role of Zooplankton Community Composition in Fecal Pellet Carbon Production in the York River Estuary, Chesapeake Bay. Estuaries and Coasts 48: 17. doi:10.1007/s12237-024-01442-8

Shatova, O., D. Koweek, M. H. Conte, and J. C. Weber. 2012. Contribution of zooplankton fecal pellets to deep ocean particle flux in the Sargasso Sea assessed using quantitative image analysis. J Plankton Res 34: 905–921. doi:10.1093/plankt/fbs053

Siegel, D. A. and others. 2021. An operational overview of the EXport Processes in the Ocean from RemoTe Sensing (EXPORTS) Northeast Pacific field deployment. Elementa: Science of the Anthropocene 9. doi:10.1525/elementa.2020.00107

Song, Y., A. B. Burd, and M. J. Rau. 2023. The deformation of marine snow enables its disaggregation in simulated oceanic shear. Front Mar Sci 10. doi:10.3389/fmars.2023.1224518

Song, Y., M. Omand, C. A. Durkin, M. L. Estapa, and K. O. Buesseler. 2025. GelCam: Visualizing sinking particle flux via a polyacrylamide gel-based sediment trap. Limnol Oceanogr Methods. doi:10.1002/lom3.10724

Stamieszkin, K., D. K. Steinberg, and A. E. Maas. 2021. Fecal pellet production by mesozooplankton in the subarctic Northeast Pacific Ocean. Limnol Oceanogr 66: 2585–2597. doi:10.1002/lno.11774

Steinberg, D. K. and others. 2023. The Outsized Role of Salps in Carbon Export in the Subarctic Northeast Pacific Ocean. Global Biogeochem Cycles 37. doi:10.1029/2022GB007523

Steinberg, D. K., C. A. Carlson, N. R. Bates, S. A. Goldthwait, L. P. Madin, and A. F. Michaels. 2000. Zooplankton vertical migration and the active transport of dissolved organic and inorganic carbon in the Sargasso Sea. Deep Sea Research Part I: Oceanographic Research Papers 47: 137–158. doi:10.1016/S0967-0637(99)00052-7

Steinberg, D. K., and M. R. Landry. 2017. Zooplankton and the Ocean Carbon Cycle. Ann Rev Mar Sci 9: 413–444. doi:10.1146/annurev-marine-010814-015924

Tarrant, A. M., N. McNamara-Bordewick, L. Blanco-Bercial, A. Miccoli, and A. E. Maas. 2021. Diel metabolic patterns in a migratory oceanic copepod. J Exp Mar Biol Ecol 545: 151643. doi:10.1016/j.jembe.2021.151643

Tomita, M., N. Shiga, and T. Ikeda. 2003. Seasonal occurrence and vertical distribution of appendicularians in Toyama Bay, southern Japan Sea. J Plankton Res 25: 579–589. doi:10.1093/plankt/25.6.579

Turner, J. T. 2015. Zooplankton fecal pellets, marine snow, phytodetritus and the ocean's biological pump. Prog Oceanogr 130: 205–248. doi:10.1016/j.pocean.2014.08.005

Urban-Rich, J., E. Nordby, I. J. Andreassen, P. Wassman, and T. Høisæter. 1999. Contribution by mezooplankton focal pellets to the carbon flux on Nordvestkbanken, north Norwegian shelf in 1994. Sarsia 84: 253–264. doi:10.1080/00364827.1999.10420430

Wiebe, P. H., A. C. Lavery, and G. L. Lawson. 2023. Biogeographic variations in diel vertical migration determined from acoustic backscattering in the northwest Atlantic Ocean. Deep Sea Research Part I: Oceanographic Research Papers 193: 103887. doi:10.1016/j.dsr.2022.103887

Wilson, S. E., H. A. Ruhl, and Jr. , K. L. Smith. 2013. Zooplankton fecal pellet flux in the abyssal northeast Pacific: A 15 year time-series study. Limnol Oceanogr 58: 881–892. doi:10.4319/lo.2013.58.3.0881

Wilson, S. E., D. K. Steinberg, and K. O. Buesseler. 2008. Changes in fecal pellet characteristics with depth as indicators of zooplankton repackaging of particles in the mesopelagic zone of the subtropical and subarctic North Pacific Ocean. Deep Sea Research Part II: Topical Studies in Oceanography 55: 1636–1647. doi:10.1016/j.dsr2.2008.04.019

Yoon, W. D., S. K. Kim, and K. N. Han. 2001. Morphology and sinking velocities of fecal pellets of copepod, molluscan, euphausiid, and salp taxa in the northeastern tropical Atlantic. Mar Biol 139: 923–928. doi:10.1007/s002270100630

Youngbluth, M. J., T. G. Bailey, P. J. Davoll, C. A. Jacoby, P. I. Blades-Eckelbarger, and C. A. Griswold. 1989. Fecal pellet production and diel migratory behavior by the euphausiid Meganyctiphanes norvegica effect benthic-pelagic coupling. Deep Sea Research Part A. Oceanographic Research Papers 36: 1491–1501. doi:10.1016/0198-0149(89)90053-8

Supplemental materials

SM1. Derivation of attenuation rates from power-law depth dependence

We assume particle abundance decreases with depth following a power law,

$$C(z) = C_0 \cdot \left(\frac{z}{z_0}\right)^{-b},$$

where z and z_o represent the target and reference depths, $C(z)$ and C_o are the corresponding abundances, and b characterizes the rate of flux attenuation. Differentiating with respect to depth gives,

$$\frac{dC}{dz} = C_0 \cdot (-b) \cdot \left(\frac{z}{z_0}\right)^{-b} \cdot \frac{1}{z} = -C \cdot \frac{b}{z}.$$

Defining the attenuation rate R as the fractional loss of particle abundance per unit time with the chain rule applied,

$$R \equiv -\frac{1}{C} \cdot \frac{dC}{dt} = -\frac{1}{C} \cdot \frac{dC}{dz} \cdot \frac{dz}{dt} = \frac{b}{z} \cdot \frac{dz}{dt}.$$

If the sinking speed is defined as $w = dz/dt$, the attenuation rate can be expressed as,

$$R = \frac{b}{z} w.$$

For a discrete estimate between two depths z_1 and z_2 with corresponding abundances (or fluxes) C_1 and C_2, the attenuation rate can be approximated as,

$$R = -\frac{1}{C} \cdot \frac{dC}{dt} = -\frac{1}{\delta t} \cdot \frac{dC}{C} \approx -\frac{w}{z_2 - z_1} \cdot \ln\left(\frac{C_2}{C_1}\right).$$

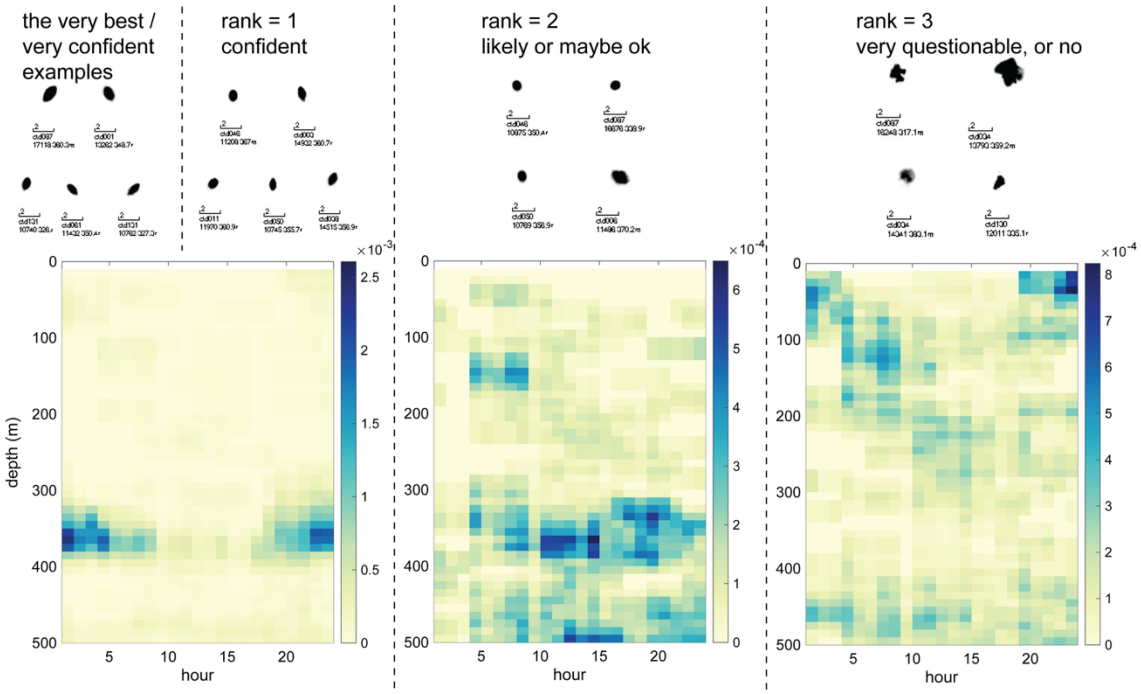

529

530 Figure S1. Classification ranks within the EcoTaxa T006 particle class. Rank 1 corresponds to
531 high-confidence identifications of appendicularian fecal pellets and represents the subset analyzed
532 in this study.

533

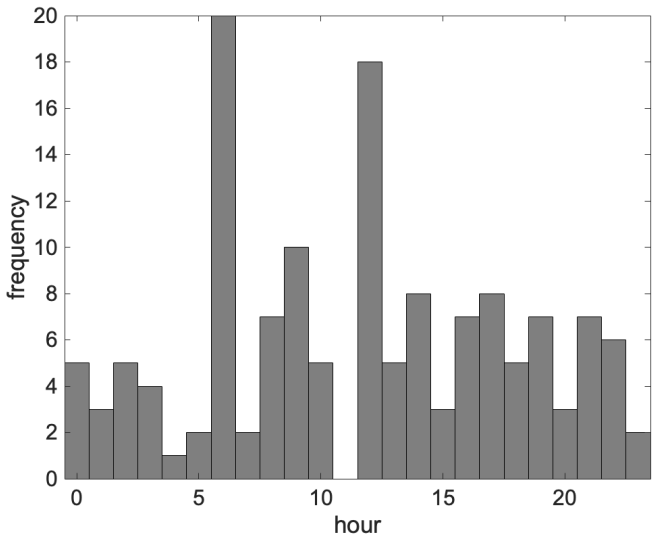

534

535 Figure S2. Number of UVP casts UVP that were included in each hourly bin (local time).

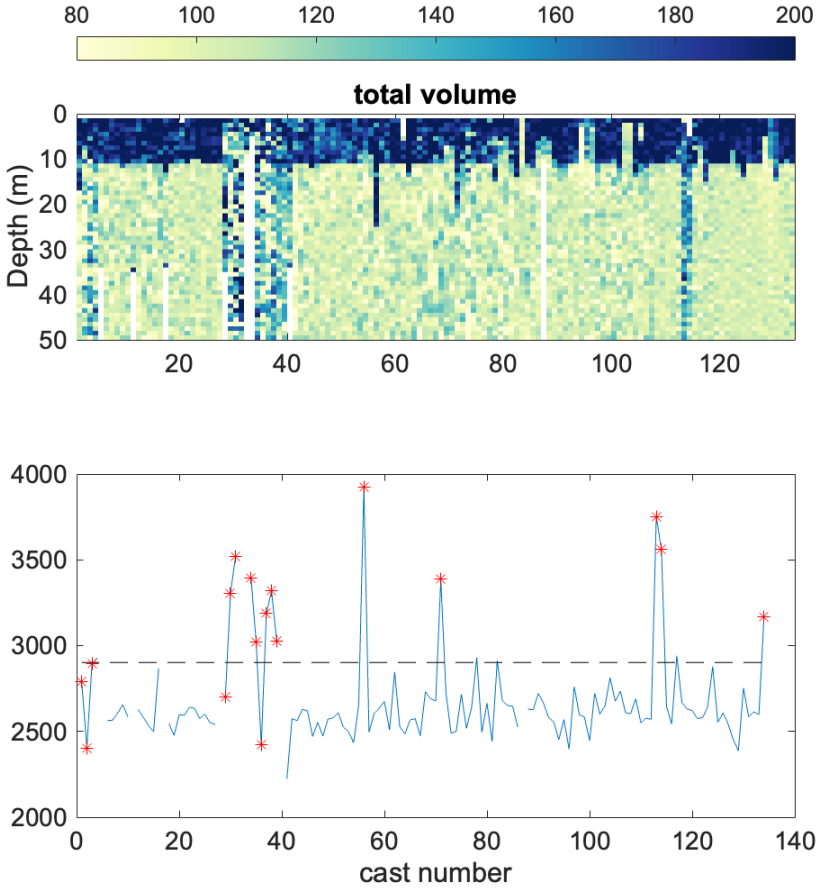

Figure S3. Total particle volumes observed by the UVP over the full sampled depth range (0–500 m). Outlier detection was based on summed particle volumes integrated from 100 to 300 m, a depth interval common to most casts, as a few profiles did not extend below 300 m. Abnormally high concentrations were identified using boxplot criteria, with outliers defined as values exceeding 1.5 × the interquartile range beyond the first or third quartile (dashed line). Casts #28–40 exhibited the largest inconsistencies; only two casts within this interval fell below the outlier threshold, but these were also excluded due to low data fidelity during this period. Test casts were excluded from all analyses.

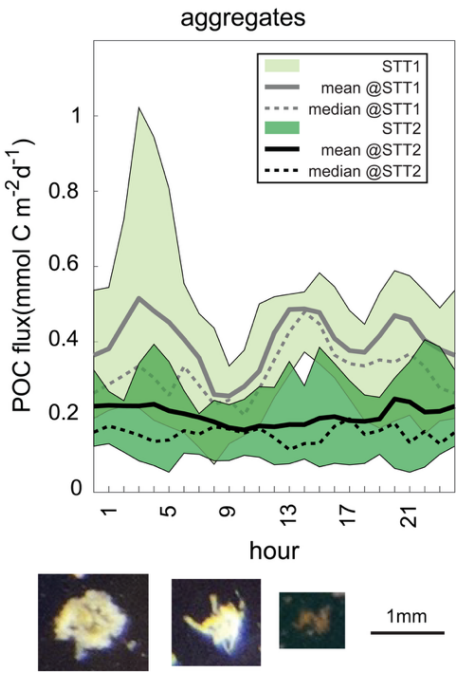

546

547 Figure S4. Time series of image derived POC proxy of aggregates by GelCam. The upper and

548 lower boundaries of the patches represent 75th and 25th percentile of the samples, with the mean

549 and median shown as solid and dashed lines.

550

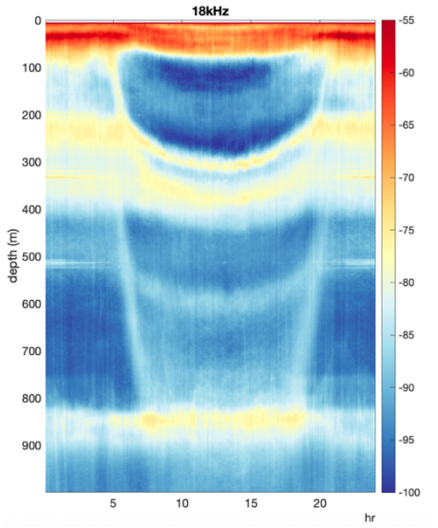

551

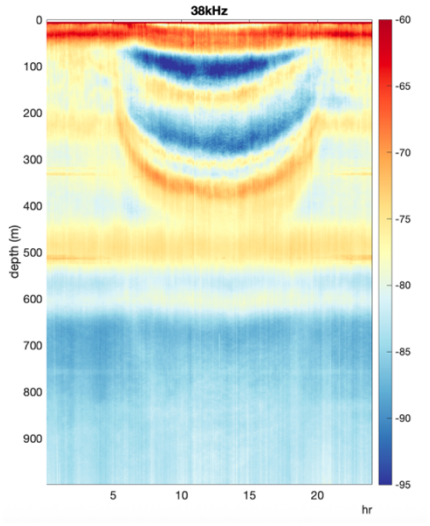

552

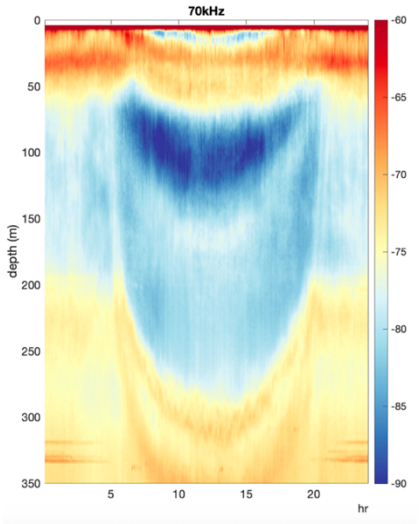

553

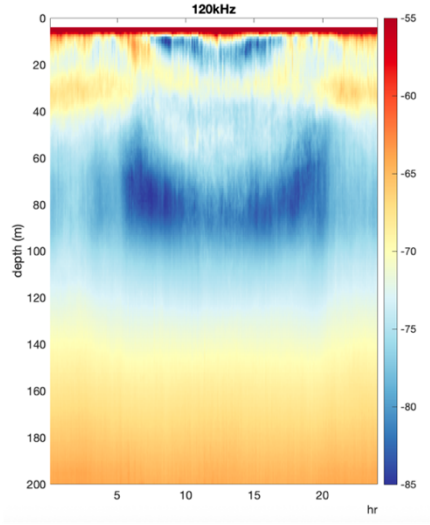

554

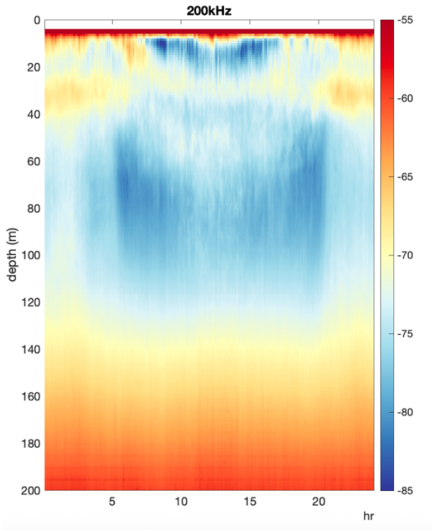

555

556 Figure S5. Averaged echo sounder signals from five channels, 18, 38, 70, 120, and 200 kHz.

557

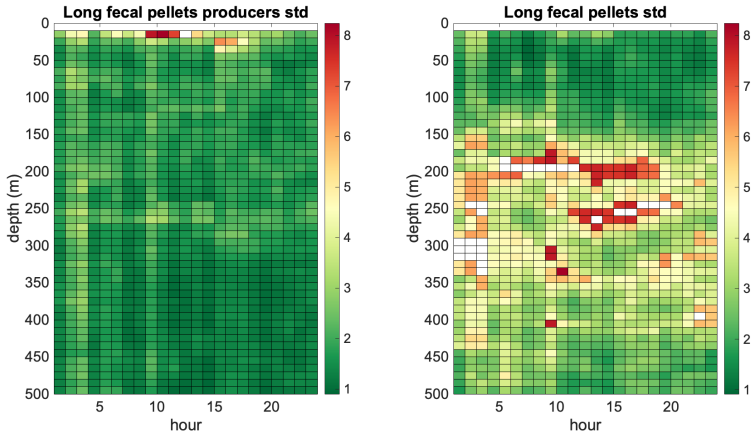

558

559

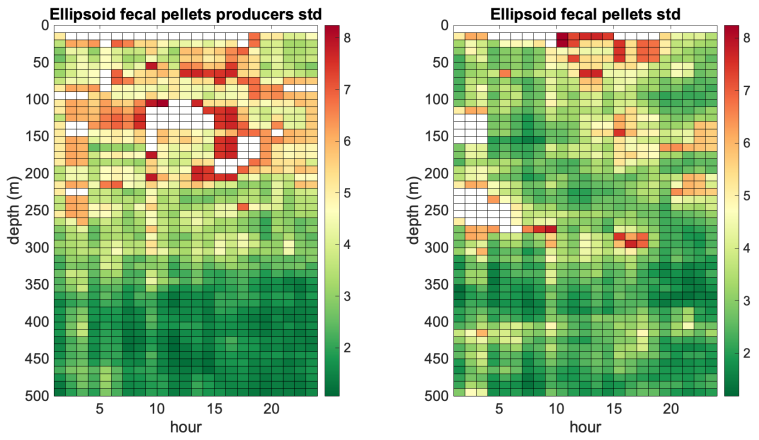

560

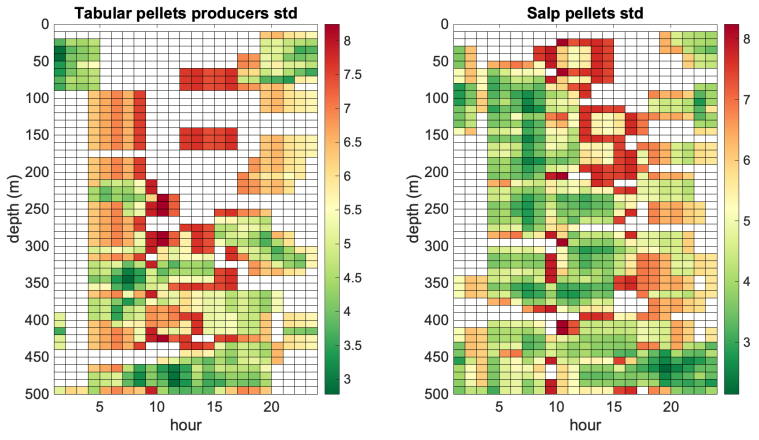

561 Figure S6. Coefficient of variation (standard deviations divided by the mean) in daily averaged
562 particle frequencies of long fecal pellets, ellipsoid fecal pellets, and tabular fecal pellets with their
563 producers through UVP measurements. The depth bin is 10 m, and the time bin is one hour.

564

565

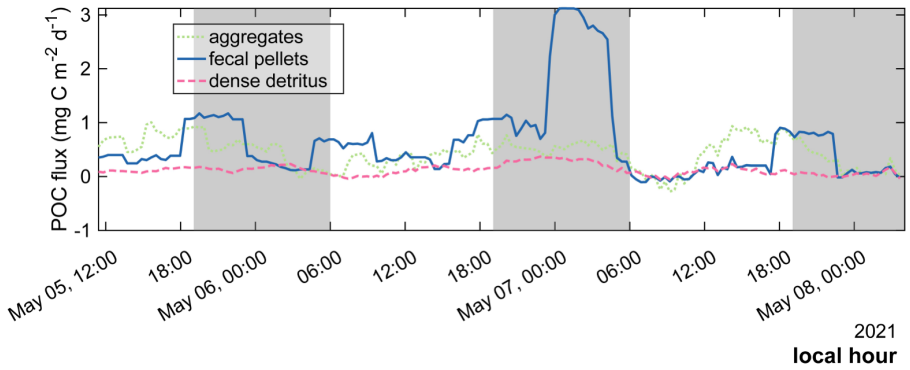

566

567 Figure S7. Time-varying POC fluxes of three particle types (aggregates in green, long fecal
568 pellets in blue, dense detritus in pink) in EXPORTS-NA. Shaded areas represent the nighttime.
569

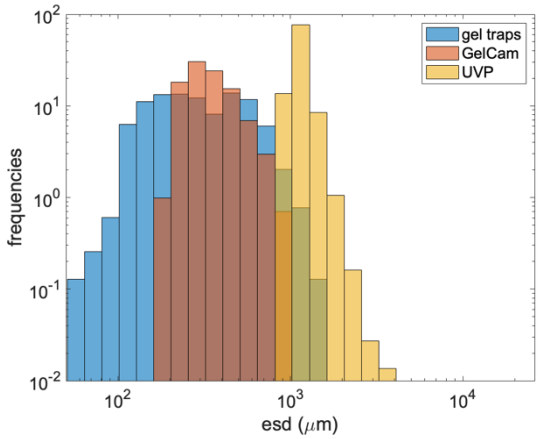

570
571 Figure S8. Particle size distributions of long fecal pellets measured by gel traps, GelCam, and the
572 UVP5. Only particles larger than 1 mm ESD exceed the UVP5 classification limit on EcoTaxa,
573 representing roughly 1 percent of all pellets collected in the gel traps.
574

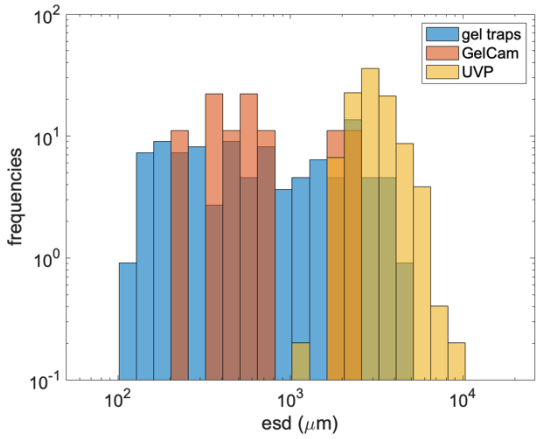

575
576 Figure S9. Particle size distributions of tabular pellets measured by gel traps, GelCam, and the
577 UVP5.
578

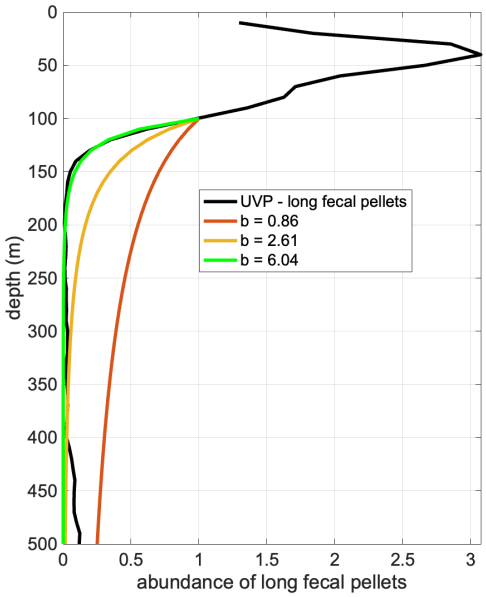

Figure S10. Vertical profiles of long fecal pellet abundance derived from UVP observations. Abundances are normalized to the value at the reference depth of 100 m. A power-law decay is fitted to the normalized profile, yielding a best-fit exponent of 6.04. Power-law exponents of 0.86 and 2.61 are shown for comparison as reference attenuation rates.